



DETECTING DEFORESTATION FROM SENTINEL-1 DATA IN THE ABSENCE OF RELIABLE REFERENCE DATA

A PREPRINT

 **Johannes N. Hansen**
School of Mathematics
University of Edinburgh
Edinburgh, UK EH9 3FD
johannes.hansen@ed.ac.uk

 **Edward T.A. Mitchard**
School of GeoSciences
University of Edinburgh
Edinburgh, UK EH8 3FF
edward.mitchard@ed.ac.uk

 **Stuart King**
School of Mathematics
University of Edinburgh
Edinburgh, UK EH9 3FD
S.King@ed.ac.uk

May 25, 2022

ABSTRACT

Forests are vital for the wellbeing of our planet. Large and small scale deforestation across the globe is threatening the stability of our climate, forest biodiversity, and therefore the preservation of fragile ecosystems and our natural habitat as a whole. With increasing public interest in climate change issues and forest preservation, a large demand for carbon offsetting, carbon footprint ratings, and environmental impact assessments is emerging. Most often, deforestation maps are created from optical data such as Landsat and MODIS. These maps are not typically available at less than annual intervals due to persistent cloud cover in many parts of the world, especially the tropics where most of the world's forest biomass is concentrated. Synthetic Aperture Radar (SAR) can fill this gap as it penetrates clouds. We propose and evaluate a novel method for deforestation detection in the absence of reliable reference data which often constitutes the largest practical hurdle. This method achieves a change detection sensitivity (producer's accuracy) of 96.5% in the study area, although false positives lead to a lower user's accuracy of about 75.7%, with a total balanced accuracy of 90.4%. The change detection accuracy is maintained when adding up to 20% noise to the reference labels. While further work is required to reduce the false positive rate, improve detection delay, and validate this method in additional circumstances, the results show that Sentinel-1 data have the potential to advance the timeliness of global deforestation monitoring.

Keywords deforestation · Sentinel-1 · change detection

1 Introduction

Accurate and timely deforestation monitoring is crucial for enabling effective prevention of deforestation and the protection of existing forest reserves. The United Nations Framework Convention on Climate Change (UNFCCC) has adopted the REDD+ (Reducing emissions from deforestation and forest degradation) rulebook to emphasize the importance of forest conservation for the halting and reversal of climate change. Developing countries under this framework are required to implement Measurement, Reporting and Verification (MRV) systems as part of a National Forest Monitoring System (NFMS). The International Panel on Climate Change (IPCC) dictates quality standards for these monitoring systems (IPCC, 2003). In particular, they must be accurate, scalable, trusted, and comparable. Furthermore, these systems are required to use remote sensing, but there are no specifications regarding the exact technologies and methods. Reiche et al. (2016) note that the majority of REDD+ member countries in the tropics are using Landsat, but no Synthetic Aperture Radar (SAR) data, for their respective MRVs. As most of these countries are subject to 70–80% cloud cover throughout the year, the use of optical data results in significant detection delays and potential blind spots. This problem can be alleviated by using SAR data which is unaffected by clouds at C-band or longer (Lu, 2006).

The capabilities of SAR for deforestation monitoring are widely demonstrated (Mitchard et al., 2011; Bouvet et al., 2018; Rahman and Sumantyo, 2010; Soja et al., 2018; Hansen et al., 2020) and Lehmann et al. (2015) have presented a strategy for combining SAR and optical data in a large-scale forest monitoring system. The lack of SAR based national monitoring systems may be due to the relative ease of optical data processing, the larger historic archives, and the comparatively limited availability of free SAR data and SAR processing tools (Reiche et al., 2016).

One of the biggest challenges in deforestation monitoring is the (un)availability of good reference data. Many detection algorithms rely on some form of supervised machine learning, and any such algorithm is only as good as its training data. The difficulty in acquiring these reference data lies in the global scale of the phenomenon, its temporal sensitivity (many detection methods may fail even a few weeks after deforestation as some vegetation has regrown), local political tension including armed conflicts, the remote location of some affected areas, and many more (Rodríguez-Veiga et al., 2017).

In practice, most reference data are generated by manually drawing polygons around areas that look like deforestation in high-resolution aerial or satellite imagery. Generally, there is a trade-off between spatial and temporal cover for any reference data set. Temporally dense data are only available over very few selected monitoring sites that may or may not be representative of forest elsewhere. Reference data of forest degradation (such as selective logging) are even more difficult to obtain. This is problematic, as according to some sources, forest degradation now accounts for more loss of biomass than deforestation (Qin et al., 2021). The most widely used global data set is published at *GlobalForestWatch* (<http://globalforestwatch.org/>). In a highly cited paper, Hansen et al. (2013) present findings from a global survey of annual forest cover, gain, and loss for the years 2000 to 2012. Their analysis is based on Landsat data, resulting in a global spatial resolution of 30 m. However, these data are not suitable for use as training data for machine learning algorithms, as they are themselves the output of a classification algorithm. The lack and quality of reference data remains an issue to be solved for deforestation monitoring. Ideally, the exact time and type of change is known for a large area. However, data of this kind are as of yet infeasible because they require continuous large scale monitoring. For global coverage, the best available forest maps are still only updated at annual intervals, including GlobalForestWatch (Hansen et al., 2013), JRC Tropical Moist Forests (Vancutsem et al., 2021), and a global forest map based on ALOS PALSAR data (Shimada et al., 2014).

In order to circumvent the reliance on reference data to train deforestation detection algorithms, one could simply apply change detection algorithms that do not rely on training labels. However, this approach has the downside that the detected changes do not necessarily correspond to deforestation but may instead reflect land cover transitions other than forest to non-forest, or indeed measurement changes that do not represent a change in the underlying land cover at all, for example: (1) seasonal changes in vegetation, (2) growth and harvest cycles in agriculture, or (3) soil moisture changes due to rainfall. This is because change detection algorithms are in no way specific to any particular type of change but merely pick up statistically significant changes in the raw data, whether or not these changes correspond to a change in the underlying state.

Mitchell et al. (2017) present an overview of existing forest degradation monitoring techniques. The authors of the review discriminate between two main approaches: (a) assessment of degradation via change in canopy cover or proxies (e.g. roads, log decks), and (b) direct quantification of loss in Above Ground Biomass (AGB). The mapping of proxies, such as the progression of forest roads or forest fragmentation, could serve as a risk assessment for potential degradation when combined with a proximity metric. In order to monitor changes in any of these metrics, a number of change detection algorithms have been developed specifically for application in remote sensing data, including BFAST (Verbesselt et al., 2010), LandTrendr (Kennedy et al., 2010), CMFDA (Zhu et al., 2012), and CCDC (Zhu and Woodcock, 2014). Vegetation indices such as Normalized Difference Vegetation Index (NDVI) and Enhanced Vegetation Index (EVI), as well as SAR backscatter are commonly used to monitor forest canopy change.

Hamunyela et al. (2017) note that the trade-off between spatial and temporal accuracy in deforestation detection is limiting the overall accuracy of disturbance maps. If short temporal detection delays are to be achieved, this typically results in low omission error but very high commission error. In particular, the use of change magnitude thresholds is seen as problematic as it relies on the assumption that true and false detections do indeed exhibit different change magnitudes. While this assumption may hold for large scale clear-felling, small scale or scattered forest disturbances may go undetected.

From these considerations we define the basic research question to be addressed in this paper. The goal is to develop a robust deforestation detection method from multivariate and multi-source data. The method should have a number of qualities: (1) It should be physics-agnostic to a reasonable degree, such that prior knowledge about the input data may improve the result, but is not required. (2) It should provide reliable deforestation alerts even in the presence of

sub-optimal reference data. (3) It should scale well with increasing dataset size. The potential for Sentinel-1 data to distinguish between forest and non-forest in a wide range of biomes has already been demonstrated in Hansen et al. (2020). In this paper, we are expanding on that study by proposing a method for detecting changes at a sub-annual timeliness.

2 Methods

The deforestation detection problem can be reframed in several different ways. For example, it can be thought of as a classification problem, where each pixel is classified as forest or non-forest at each time step. Deforestation events would then be declared wherever a pixel changes class from forest to non-forest between consecutive time steps. This approach has several downsides: firstly, it requires reliable reference data that are both temporally and spatially accurate for training the classifier. In addition, it is not very robust because different land cover classes may look very similar to forest at some time steps, either because of random fluctuations (speckle, noise, etc.) or because of seasonal effects (greening and senescence in forests; growth and harvest in agriculture). This approach would therefore likely detect a multitude of changes back and forth between classes.

Alternatively, we can directly apply off-the-shelf change detection algorithms to the time series data. This is problematic for similar reasons as the previous approach, mainly because a change in the time series behavior does not necessarily indicate a change in land cover, and vice versa.

In our case, we want to think about a deforestation event as a deviation of the pixel from the reference class (stable forest). We therefore want to detect the point in time when the pixel time series starts to be dissimilar to the characteristic forest time series. This requires a time-dependent measure of similarity between the two time series. Because of this, we convert the original time series into another time series that characterizes how dissimilar the pixel is to forest at that time. The original change detection problem is then transformed into the task of detecting an increase in forest dissimilarity.

2.1 Study Site and Reference Data

For developing and testing the method we chose a small site near Paragominas in Pará, Brazil, that exhibits very clear deforestation in large patches for the years 2017, 2018, and 2019. Figure 1 shows a series of Sentinel-1 images for this study site, in approximately six-month intervals. In addition, fig. 2 shows high-resolution optical data for the same area, provided free of charge by Planet through the NICFI program (NICFI, 2021). The dates shown for the Sentinel-1 images were chosen to approximately correspond to the available NICFI images.

Figure 3 shows the annual forest loss events for the study site obtained from two reference data sets: (1) The GlobalForestWatch dataset (Hansen et al., 2013) and (2) The Tropical Moist Forests product provided by the EC JRC (Vancutsem et al., 2021). In addition, fig. 3c shows a manual segmentation of the study site into polygons that exhibit roughly synchronous behavior throughout the time period. This way, one date of change can be assigned to each area, although some of these areas are deforested in a rainbow pattern, i.e. the change spans a period of time that typically covers a few Sentinel-1 images. The change dates shown in the figure were derived from visual interpretation of Landsat-8 data and represent the latest possible date that the deforestation has likely occurred. Because of extensive cloud cover in the area, it is possible that the forest loss happened earlier but could not be detected until the date shown. The change detection results will be evaluated with respect to these three maps.

2.2 Change Detection

As described earlier, the accuracy of deforestation detection methods is hindered by the scarcity and low quality of reference data, as well as the fact that traditional change detection methods may pick up changes corresponding to events other than forest loss. To solve these problems, and to mitigate the disadvantages of both the fully supervised and the fully unsupervised methods, in this paper we are demonstrating a partially supervised approach: Instead of requiring reference data that capture land cover changes and therefore need a temporal component, we have developed a method that only relies on a stationary forest map and thus classifies pixels as either being stable forest or not. Pixels that are not stable forest could include agriculture, urban areas, other forms of vegetation, etc., or pixels that undergo deforestation at some point.

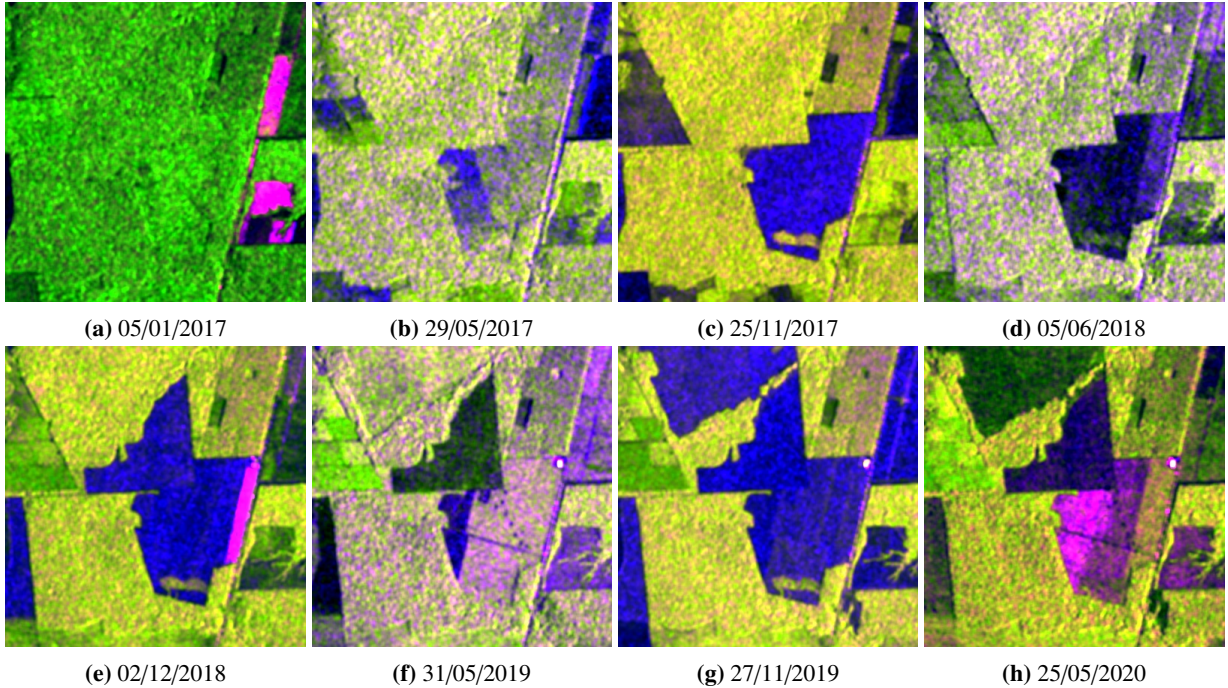


Figure 1: This figure shows a series of Sentinel-1 images of the study site in Paragominas, Brazil, during the period 2017–2020. The RGB channels represent the backscatter in VV, VH, as well as their ratio VV/VH.

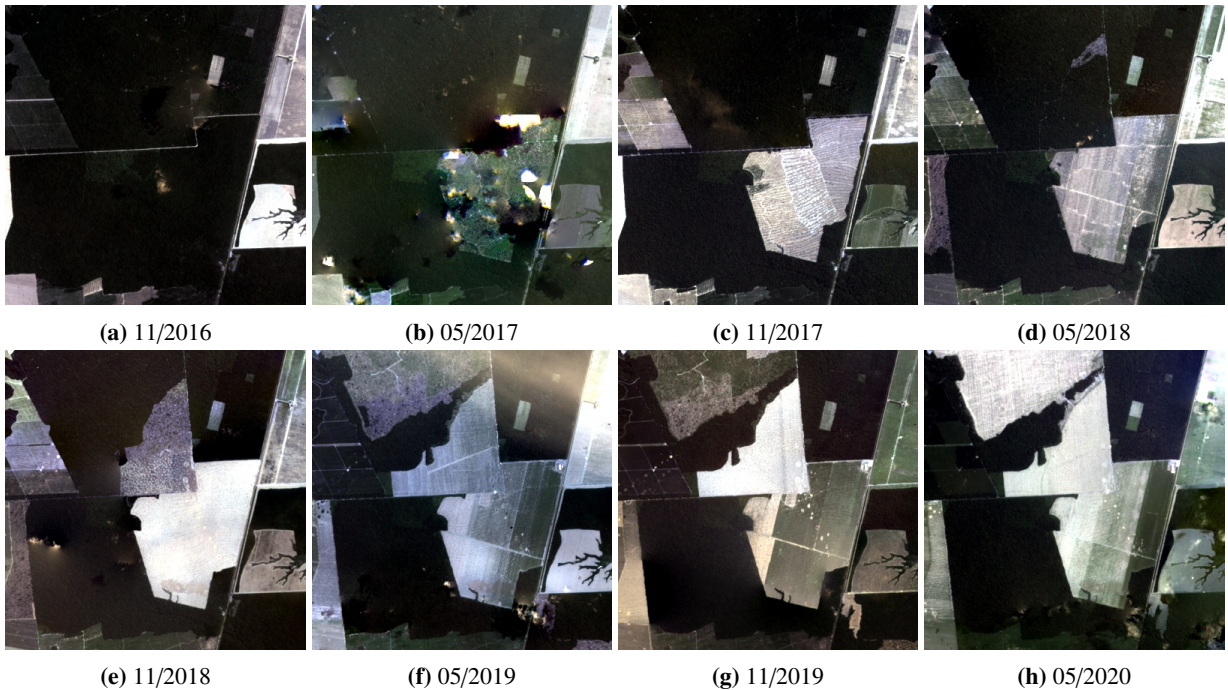


Figure 2: This figure shows a series of six-monthly RGB composites of the study site in Paragominas, Brazil, during the period 2017–2020. The images are provided by Planet via the NICFI program (NICFI, 2021).

This reference forest map can then be used to detect pixels that deviate from the reference class. This is done by computing a similarity measure between the time series of the pixel and the reference forest time series. The similarity can then be computed over time and compared to the expected similarity if the pixel was forest. Transitions from forest to non-forest can then be recorded as a drop in forest similarity above a set threshold.

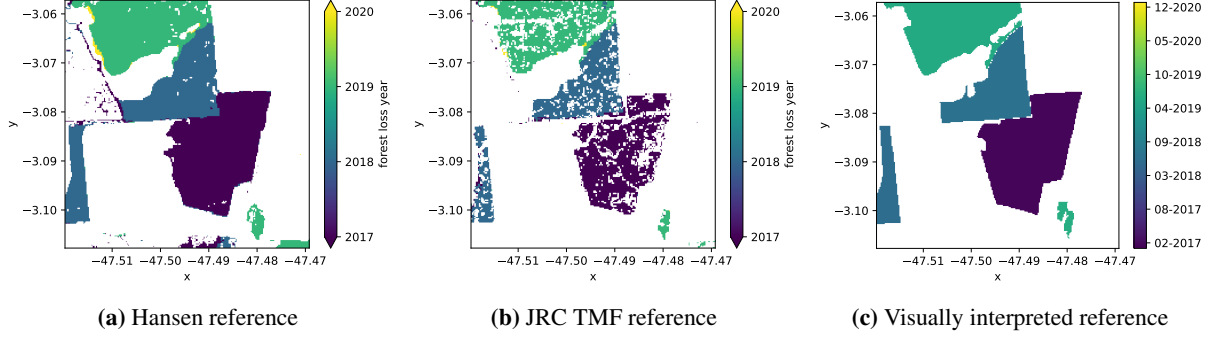


Figure 3: Reference change maps. The colored pixels indicate the year of forest loss, whereas white pixels indicate no change, which includes stable forest as well as non-forest.

The changepoint detection is simplified by the fact that there is only one type of change of interest — forest to non-forest — and that there is a maximum of one such change in the time series. We therefore do not need to worry about detecting multiple changes. The change detection method is based on the following steps:

1. Obtain an initial reference forest mask. This could be based on Hansen et al. (2013) or any other forest dataset. It does not need to be exhaustive or multitemporal but should cover areas that remain stable forest throughout the time period.
2. Based on the data and the reference mask, compute the reference data distribution for forested areas at each time step by creating a histogram of the masked data. Let $b(x_{i,t})$ denote the histogram bin and $C_{b(x_{i,t})}$ the histogram count at that bin.
3. From the forest histogram, compute the forest similarity for each pixel at each time step t , for each variable i :

$$p_{i,t}(x_{i,t}) = \frac{1}{\sum C} C_{b(x_{i,t})} \quad (1)$$

with $p_{i,t}$ being the forest similarity at time step t , given the value $x_{i,t}$ for variable i . In this case, the variables are the co-polarized and cross-polarized backscatter (VV and VH). However, the method generalizes to any multivariate data.

4. To combine the similarities from all available variables into a univariate time series, we compute the joint forest similarity as:

$$p_t(x_t) = \prod_i p_{i,t}(x_{i,t}) \quad (2)$$

5. For comparison with the expected similarity values if a pixel is forest, we compute the same joint similarity for forest pixels and use the q -th quantile $p_t^{F,q}$ as threshold for declaring a pixel non-forest (this means that a fraction q of forest pixels would also be declared non-forest at this stage).
6. Compute the cumulative product of the similarity threshold ratio:

$$\Lambda_t(x) = \begin{cases} 1 & \text{if } p_{t-1}(x) < p_{t-1}^{F,q} \\ p_0(x)/p_0^{F,q} & \text{else if } t = 0 \\ P_{t-1}(x) \cdot p_t(x)/p_t^{F,q} & \text{else} \end{cases} \quad (3)$$

$\Lambda_t(x)$ increases as consecutive time steps fall above the threshold $p_t^{F,q}$ and is therefore a measure of confidence that the pixel is in fact non-forest at this time step.

7. Set a threshold L for Λ_t for the pixel to be considered non-forest.
8. Finally, a deforestation event is declared at time step T if $\Lambda_T(x) \geq L$ and $\Lambda_t(x) < L \forall t < T$.

For noise reduction, a non-local means filter was applied to the spatio-temporal datacube (Buades et al., 2011) (implemented in Hansen (2022)). Figure 4 demonstrates how an initial forest mask can be used to compute the distribution of feature values for the forest class (steps 1 and 2). The forest mask for this demonstration was obtained from visual interpretation (see fig. 6b), but would in general be an existing forest map of uncertain quality. In this case, the distribution of forest backscatter values looks nearly Gaussian (as indicated by the Gaussian curve fit), but this need not be the case in general.

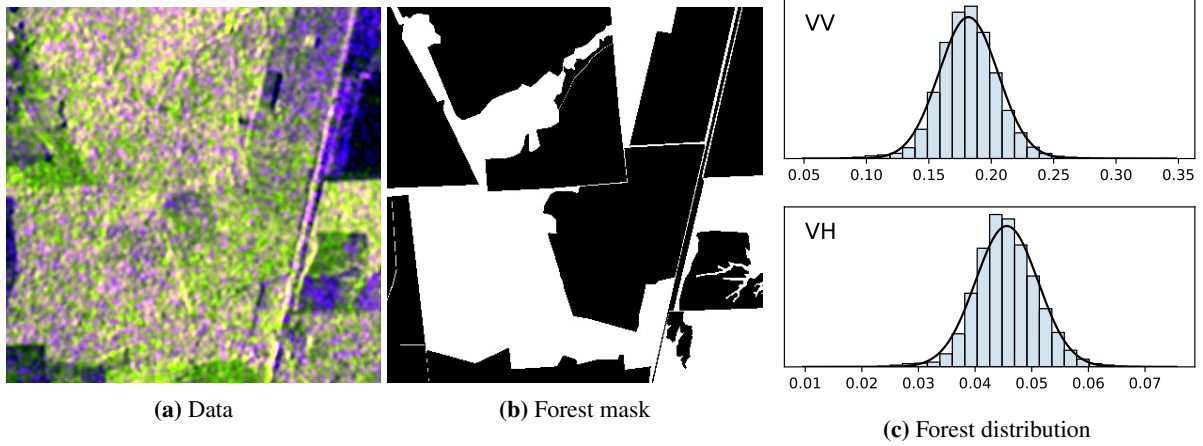


Figure 4: This figure shows a time slice of Sentinel-1 data for the study site in Paragominas, Brazil (fig. 4a), a mask showing the areas of stable forest throughout the study period (fig. 4b), and the distribution of VV and VH values for the forest class based on the forest mask (fig. 4c).

Figure 5 shows a demonstration of the change detection method for two sample time series. The top two graphs show the time series of the VV and VH values of each pixel (in orange), along with the forest mean (in blue). 98% of all forest pixels fall within the light blue band. The bottom plots show the forest similarity $p_t(x_t)$ measure in black, and the cumulative similarity $\Lambda_t(x)$ as a dashed red line. The areas shaded in red indicate those parts that are considered non-forest based on the threshold L . The first time series (fig. 5a) is of a pixel that undergoes deforestation early on in the time period. This event is detected at the start of first shaded area. The second time series (fig. 5b) shows a non-forest pixel that looks similar to forest for large parts of the time series.

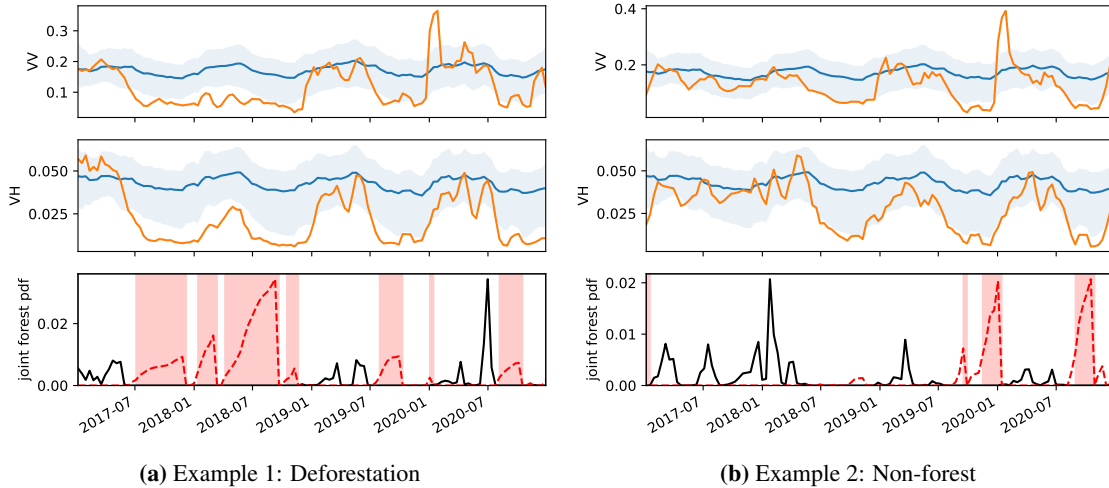


Figure 5: Change detection demonstration for two sample pixels. The time series of the pixels for VV and VH is shown in orange, the reference forest time series is shown in blue (with a light blue band marking the 1st-99th percentile within the forest class). The third row shows the joint probability density for the pixel being forest at each time step as a black line. The dashed red line shows our measure of certainty $\Lambda_t(x)$ for the area being non-forest, and the light red areas show such times where the non-forest certainty exceeds a set threshold. A deforestation event is then declared at the first encounter of a red area.

2.3 Accuracy Assessment

In general, there are two metrics of interest when assessing the accuracy of any change map: the *spatial* accuracy and the *temporal* accuracy. The spatial accuracy encompasses the precision and recall with which changes are detected in

a binary classification setting, i.e. the classification of change vs. no change (independent of the time of change). The temporal accuracy is a measure of the accuracy of the detected time of change. This can be measured as the mean delay of the detected change or the root mean square error (RMSE) of the change time.

While the spatial accuracy can be directly computed from the reference data shown in fig. 3, the temporal accuracy can only be quantified in a meaningful way when the precise date of change is known. The output of the change detection algorithm will always be a precise time of change that can easily be reduced to a year of change. However, while comparing the year of change can give some general insight into the temporal accuracy, it is not a sufficient measure of the uncertainty in the time of change. Not only is comparing the year of change a less accurate measure than comparing e.g. the month of change, it is in fact qualitatively different: if the true year of change for one pixel is 2017 but the detected change is for January 2018, we do not know if this indicates a delay of only one month—which may be an acceptable detection delay—or a whole year, in which case the difference is not merely a delay but likely the detection of an entirely different change, i.e. a complete miss of the original first change. Instead, we are only going to compute the mean time lag with respect to the visually interpreted data as a rough indicator of the temporal accuracy, while acknowledging that better reference data are necessary for a true quantification of this uncertainty.

The spatial accuracy is computed by reducing the change result to a binary map (change / no change). Several accuracy measures are commonly used for assessing such a map. All of these can be computed from the entries of a confusion matrix, i.e., the number of true positives (TP), true negatives (TN), false positives (FP), and false negatives (FN). The Producer’s Accuracy (PA) (also known as sensitivity, recall, or true positive rate) in this context is the probability that an actual change is accurately detected. It is defined as

$$PA = \frac{TP}{TP + FN} \quad (4)$$

The User’s Accuracy (UA) (also known as precision or positive predictive value) is defined as the probability that a change shown on the map corresponds to a true change on the ground. It is given by

$$UA = \frac{TP}{TP + FP} \quad (5)$$

The Overall Accuracy (OA) (or simply accuracy) is defined as

$$OA = \frac{TP + TN}{TP + FP + TN + FN} \quad (6)$$

and is the overall fraction of correctly classified pixels as change or no change. The OA can be a misleading accuracy measure as it depends on the fraction of pixels that are subject to change. A more robust measure is the Balanced Accuracy (BA) which accounts for class imbalances, i.e., the case where the available classes have different numbers of members (Broderson et al., 2010). It is defined as

$$BA = \frac{1}{2} \left(\frac{TP}{TP + FP} + \frac{TN}{TN + FN} \right). \quad (7)$$

3 Results

Figure 6 shows the result of the algorithm for the site in Paragominas, Brazil (fig. 4) for a time series from 2017–2020. The change detection delay in days is shown in fig. 6c. This is computed with respect to the true deforestation dates as extracted via visual inspection of Landsat and Planet data (fig. 6b).

A comparison of the resulting change map (fig. 6a) with the reference map from visual interpretation (fig. 6b) shows that all areas of deforestation are picked up reliably. In addition, however, deforestation is falsely detected in several areas where in fact no deforestation is happening. All of these are areas that have undergone deforestation in the past. For example, the patch in the north-western corner of the area is being picked up as deforestation, when in fact it was non-forest even at the start of the time series. The backscatter signature of these areas looks very similar to that of forest at the start of the time series, such that the algorithm is confused into detecting a transition from forest to non-forest when in reality the pixel was non-forest throughout the time period. The achieved PA is 96.5%, with a UA of 75.7% and a balanced accuracy of 90.4%, reflecting these findings.

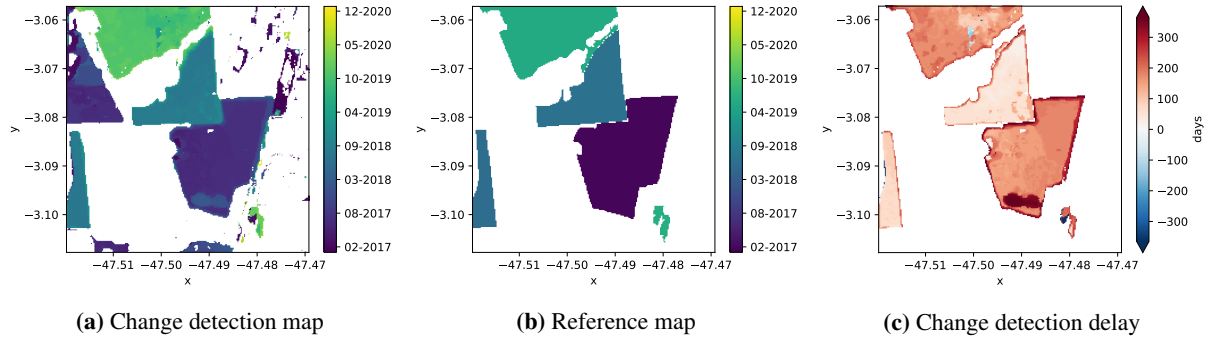


Figure 6: This figure shows a comparison of the detected date of change (fig. 6a) and the reference map obtained from manual interpretation (fig. 6b). For those pixels where both maps indicate a change, fig. 6c shows the change detection delay in days.

Figure 7 shows the mean time series for some of the polygons delineated in fig. 3c. The solid blue line indicates the forest reference time series, with the light blue band marking the 1st–99th percentile of forest pixels. In addition, the mean change point is indicated for each polygon, along with the standard deviation (marked as vertical gray band around the change point). The opacity of the marked change point and its uncertainty is scaled with the fraction of pixels in the area for which a change point was detected.

The first row represents stable forest. While changes are detected for some pixels in this area, e.g. due to imperfect polygon boundaries, the algorithm only produces very few false positives over forested areas, as visually indicated by the low opacity of the marked mean change point. On the other hand, the third row is an examples of an area that is non-forest throughout the time period, but is consistently classified as deforestation events using the method shown. The third row in particular, and also the sixth and last row, are non-forest but look very similar to forest in their temporal radar signature, confusing the algorithm into mistakenly predicting deforestation — illustrating the reason for the false positives detected in the change map above.

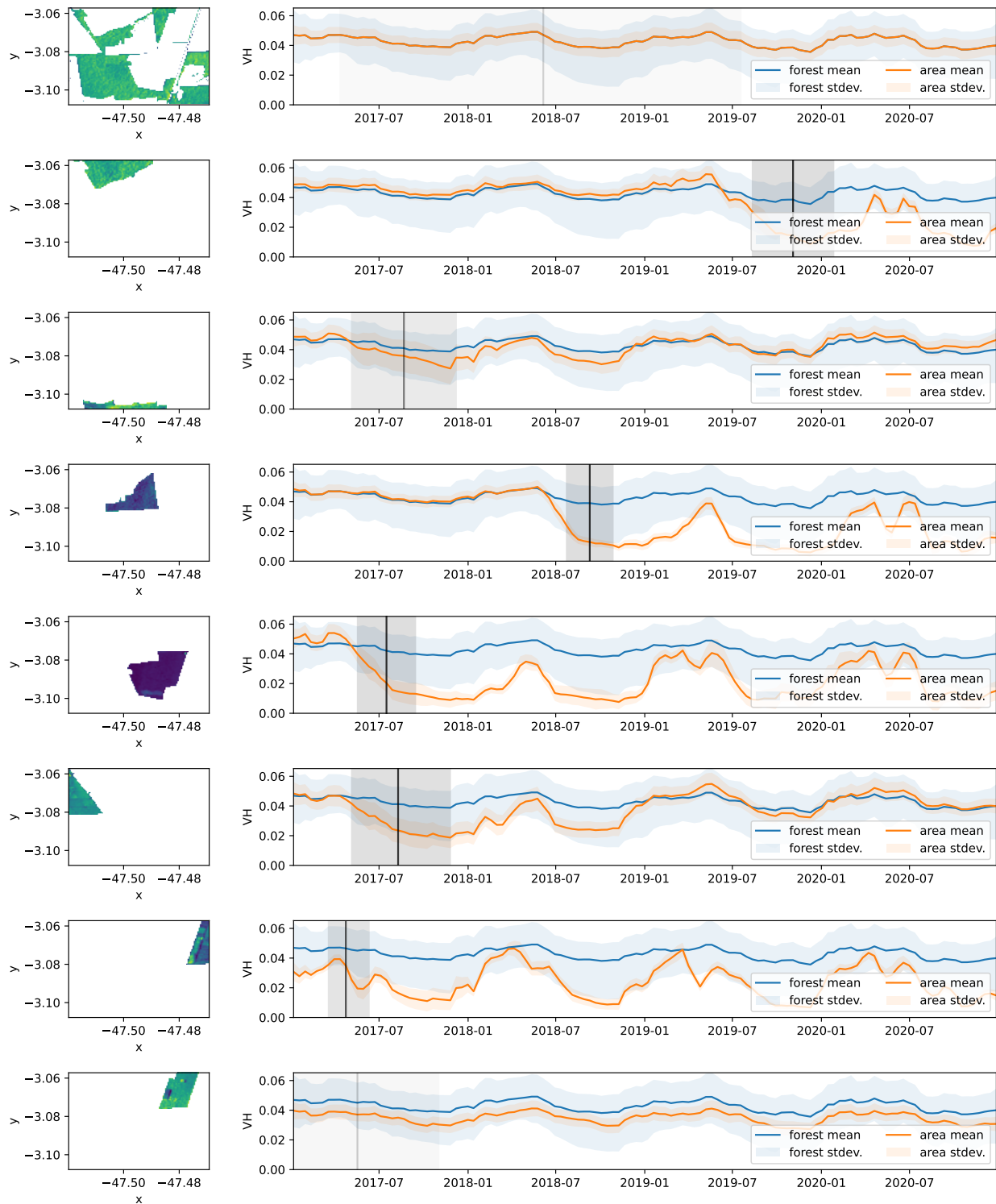


Figure 7: This figure shows the mean time series for some of the polygons shown in fig. 4b. It also shows the mean change point detected for this area as a vertical gray line. The change point variation in the area is shown as a gray band around this line. The opacity of the change point line indicates the fraction of detected change points – for the first and last row, for example, change points were only detected for a small number of pixels. The blue line and light blue band indicate the reference forest time series mean and 1st-99th percentile, respectively.

3.1 Validation at additional sites

To validate that the method works in diverse biomes and conditions, it was tested on three additional sites with distinct deforestation and vegetation change patterns. The sites chosen are located in (1) Porto Velho, Brazil (2017–2021), (2) South Cameroon (2017–2018), and (3) Riau, Indonesia (2020–2021). Figure 8 shows an individual Sentinel-1 image as well as a NICFI (NICFI, 2021) RGB composite for each of the sites.

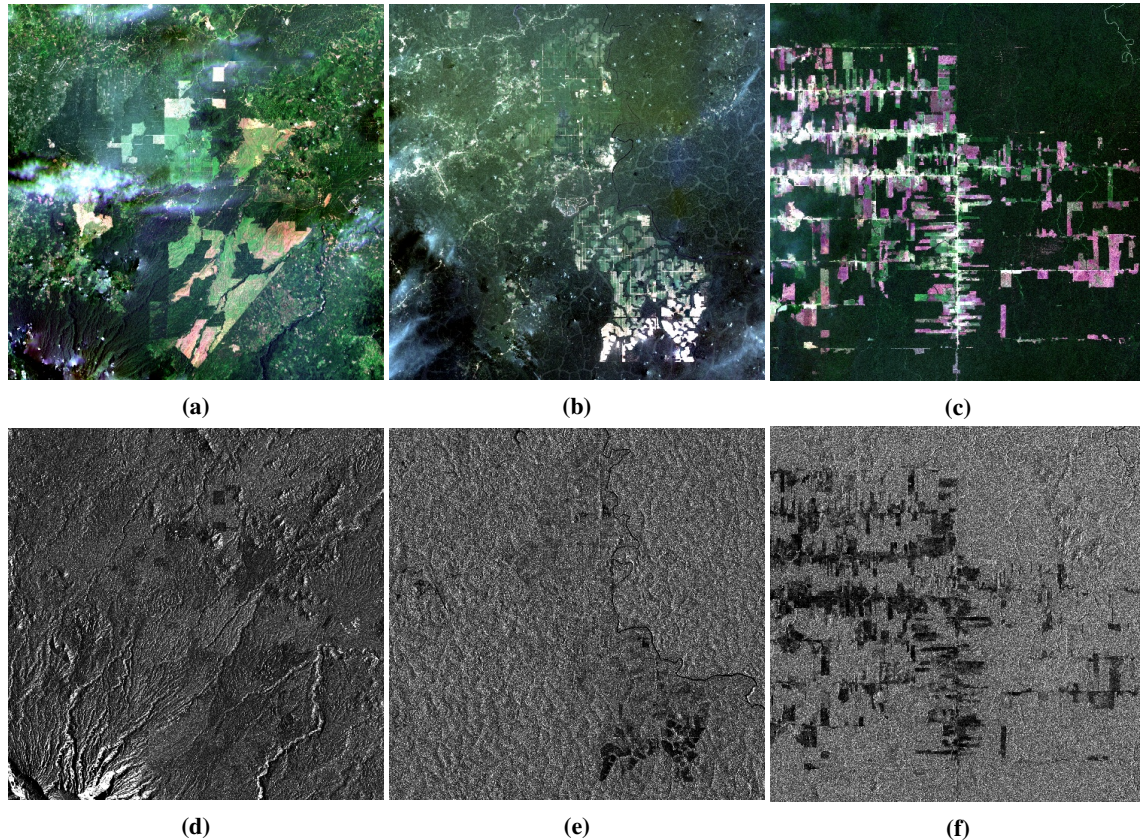


Figure 8: This figure shows individual Sentinel-1 images (VV) and NICFI images of the same time period for comparison, for each of the additional validation sites. The images shown are for Riau, Indonesia (October 2021, figs. 8a and 8d), Cameroon (December 2018, figs. 8b and 8e), and Porto Velho (figs. 8c and 8f).

It is immediately evident that the deforestation is harder to detect with Sentinel-1 than with optical sensors. While deforestation can be clearly observed in Brazil and partially also in Cameroon, the deforested patches in Indonesia are almost invisible to the eye in the Sentinel-1 image. Detection is further complicated by the presence of mountainous regions in the south western corner. The resulting change detection output is shown in fig. 9. The maps on the left show the change detection results, the middle maps are the Hansen reference (Hansen et al., 2013), and the maps on the right are the JRC TMF deforestation maps (Vancutsem et al., 2021). For these sites, no deforestation reference was extracted by visual interpretation. For that reason, only the year of change is known from the two reference maps. The reference maps therefore show discrete change years, while the change detection map on the left shows a continuous change date as indicated by the more graduated color scheme.

In addition to being able to provide an actual date of change for each deforestation event, it is apparent from the Cameroon maps that the Sentinel-1 based change maps are not affected by the stripy Landsat artifacts that are apparent in both the Hansen and JRC maps. However, there are also limitations that are evident in the resulting change maps. For example, the change maps appear to be generally noisier than the reference maps. This noise may be partially due to false positives in non-forest areas as discussed previously, but may also be an artifact of the Sentinel-1 data used. While Sentinel-1 data can definitely separate forest and non-forest when aggregated annually, separation at an individual time step is unreliable because of speckle and seasonality (Hansen et al., 2020). Optical data are generally better suited for differentiating these classes at a single time step, assuming a cloud-free image. Therefore, a direct

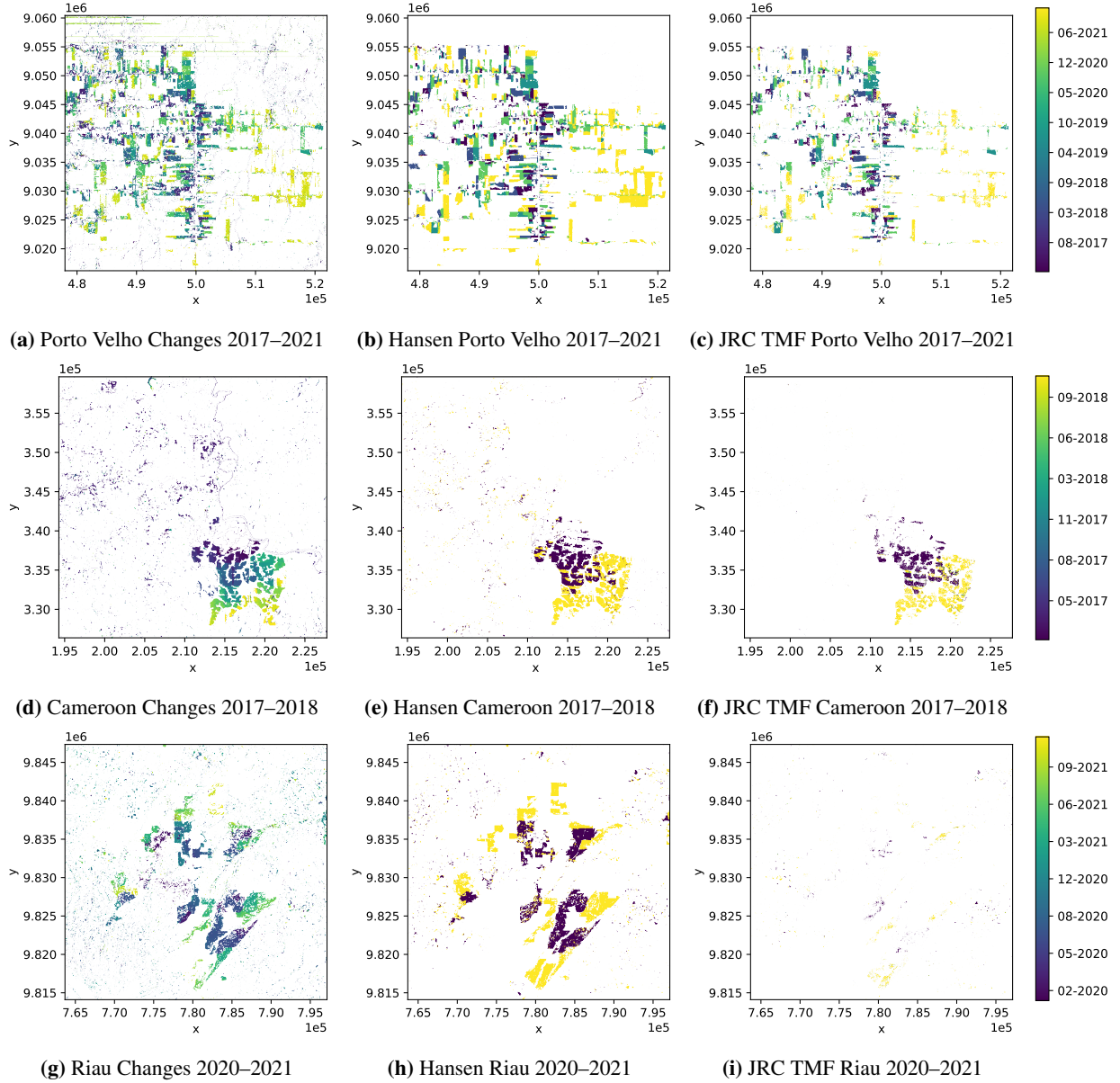


Figure 9: This figure shows the deforestation maps obtained at three additional validation sites, along with the reference maps from Hansen et al. (2013) and Vancutsem et al. (2021).

comparison between a day-by-day change map from SAR data and an annual map from optical data in terms of spatial noise is an unfair comparison as the annual map can be considered to have applied a large amount of temporal smoothing to eliminate noise and at the same time get around the problem of missing data.

Table 1 summarizes the accuracy metrics computed for each site with respect to the various available reference maps. It shows the UA, PA, and BA (see section 2.3). The thresholds q and L were chosen to optimize the BA with respect to the Hansen maps.

The accuracy scores show some variance between the sites. It is evident that the method generally achieves a high PA, potentially at the cost of a lower UA. The lower UA is driven by the false positives observed. The most reliable accuracy scores are those based on the visual interpretation, as the Hansen and JRC maps carry errors in themselves and do not necessarily reflect the ground truth. This is particularly evident for the JRC based accuracy scores for the Indonesian site. These scores are very low as the JRC map fails to detect any deforestation in this area. These issues

Table 1: This table summarizes the accuracy metrics UA, PA, and BA for each site, with respect to the Hansen and JRC maps, as well as a visual interpretation in the case of the Paragominas site.

Reference	Site	UA	PA	BA
Hansen	Paragominas	77.7%	86.5%	85.5%
	Cameroon	48.0%	67.7%	81.4%
	Riau	49.8%	61.0%	76.9%
	Porto Velho	62.0%	76.4%	83.2%
JRC	Paragominas	57.9%	91.7%	83.6%
	Cameroon	34.9%	82.2%	88.1%
	Riau	5.3%	48.3%	68.0%
	Porto Velho	42.9%	84.0%	85.0%
Visual	Paragominas	75.7%	96.5%	90.4%

serve to illustrate the fact that the accuracy scores do not fully reflect the performance of the change detection method. The method may in fact outperform the Hansen and JRC maps, in which case a lower score would reflect negatively on these reference maps instead. However, they do serve as a useful sanity check of the results.

Indonesia is a challenging site as the forested areas look very similar to the non-forest areas in the backscatter (see fig. 8). It also exhibits more terrain than the other two sites, further complicating the use of SAR data. In general, balanced accuracy scores of about 80% were observed with respect to both the Hansen and JRC maps. The PA and UA scores vary strongly between sites. The UA is generally low due to the number of false positives. The PA is as low as 60–70% for Indonesia and Cameroon (compared to Hansen), and as high as 80–90% for the two Brazilian sites.

3.2 Noisy reference labels

Given that the idea behind this method is to be relatively independent of high quality training data, in this section the behavior of the method in the presence of mislabeled data is investigated. To simulate corrupted training data, a forest reference ensemble of size N is generated for a range of fractions c of incorrectly classified forest pixels such that $(1 - c)N$ ensemble members are true forest pixels, and cN ensemble members are in fact non-forest. For each such corrupted reference ensemble, a change map was generated and the corresponding accuracy values were computed.

Figure 10 shows these maps of detected change for fractions between 0% and 22%. Up to about 10% incorrectly classified pixels, there is no major visible degradation of the change map. At higher percentages of corruption, changes that occur later in the time series are the first to be missed. However, a large amount of true changes are still detected up to 22% corruption. Furthermore, the corruption of the training data only increases the error of omission (the number of missed deforestation events), but not the commission error (the number of false positives). These findings are corroborated by a graph of the accuracy scores (UA, PA, and OA) as a function of the corruption fraction in fig. 11. The accuracy scores are computed with respect to the visually interpreted change reference (fig. 3c). The PA is decreased significantly above 10% corruption, but the UA does not significantly decrease – in fact, it increases slightly initially as the overall number of detected changes is reduced, including previous false positives. As a consequence, the OA does not deteriorate significantly even at 20% corruption. However, the PA is arguably the most important metric as the correct identification of all deforestation events is the primary goal. As stated previously, the false positives mostly occur in areas of non-forest and could be removed by other means, e.g. by comparing the results with optical data where non-forest areas may have been apparent even at the start of the time series.

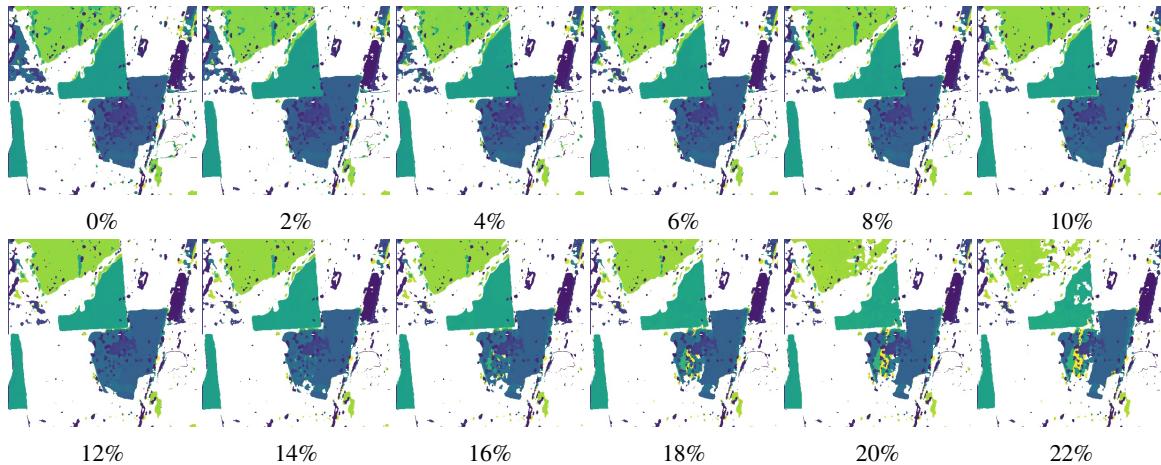


Figure 10: This figure shows change maps for various levels of training data corruption. The percentages indicate the fraction of pixels in the forest reference mask that are in reality non-forest pixels.

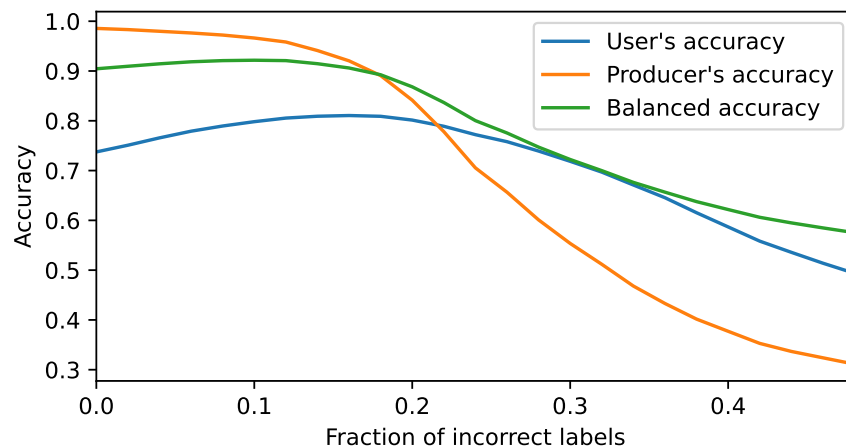


Figure 11: This graph shows the effect of training data corruption on the change detection accuracy. The UA, PA, and OA are shown as a function of the fraction of incorrect labels.

4 Discussion

We have shown in the preceding sections that the proposed method is very successful at picking up deforestation events in diverse environments by quantifying the deviation from a reference class characterized by a static reference map. This is true even in adverse conditions such as the site in Indonesia, where deforestation is hard to make out from Sentinel-1 data even by visual inspection. Statistically significant change deviations are reliably picked up, resulting in a small false negative rate.

We have already touched upon possible limitations of the method. Firstly, there are cases where the backscatter signature of non-forest areas is very similar to forest areas temporarily. Nearly all false positives occur in such areas, when the backscatter is similar to forest at the start of the time series. Consequently, all of these false positives are detected at dates near the beginning of the time period. These commission errors can be reduced by extending the time series into the past and reserving the first e.g. six months to ascertain which areas were forest initially.

However, much of these shortcomings may in fact be due to the inadequacy of Sentinel-1 data for the deforestation detection task. It would therefore be useful to explore this method with additional data sources. As the proposed method is entirely agnostic to the type of input data, it can also be applied to other SAR sensors and optical data, even in combination with Sentinel-1 as it supports multivariate data.

Another issue with this method and Sentinel-1 is the sensitivity to terrain. As terrain has a big impact on SAR backscatter values, backscatter deviations from the reference class in areas with uneven topography may occur due to deviations in terrain rather than deviations in the actual land cover. This was observed in part of the Indonesian site, where a mountain in the south western corner caused false positives. This could potentially be addressed by appropriate terrain flattening, or including optical data that are less sensitive to terrain.

It is also worth noting that this method is not specific to deforestation, but can be applied to any use case where changes from some reference class need to be detected. This includes applications in agriculture, e.g. detecting harvesting when only a map of agricultural fields in the region is known.

5 Conclusions

The development of this change detection method was motivated by some of the biggest challenges around deforestation detection using SAR data, in particular (1) the lack of reliable reference data and (2) the fact that changes in backscatter need not represent changes in land cover/use. We have shown in this paper that some of these challenges may be addressed with a semi-supervised approach where changes are detected with respect to the prototype time series of a reference class. This prototype time series captures the natural variability of the forest backscatter signature and removes the potential for mistakenly detecting changes due to other effects. In addition, this method works with noisy reference data as it is robust to outliers present in the reference class ensemble, with no significant degradation of the results up to about 10–20% reference data corruption. By detecting changes as deviations from a single reference class rather than by classifying between two possible classes, we remove the need to parametrize the non-forest class. This is advantageous for generalizing the method as the non-forest class is inherently heterogeneous and may include many different land cover types.

While the results from this method do not necessarily outperform the reference maps in terms of spatial accuracy, they do provide an actual date of change rather than just a year which is advantageous for near-real-time forest monitoring systems and critical for actionable insights. They change maps can also be generated from static reference maps without requiring noise-free reference data. In this way, the method can be thought of as a means to iteratively improve existing change maps.

In conclusion, Sentinel-1 SAR data are certainly capable of detecting deforestation, even though a longer time series may be required to reliably tell apart forest and non-forest – potentially limiting the temporal change detection accuracy. There is no doubt that more innovations are possible in the field of multi-sensor fusion – combining the advantages of SAR, lidar, and optical data – and the use of spatial features for separating forest and non-forest with even shorter time series.

References

- Bouvet, A., Mermoz, S., Ballère, M., Koleck, T., Le Toan, T., 2018. Use of the SAR shadowing effect for deforestation detection with Sentinel-1 time series. *Remote Sensing* 10, 1–19. doi:doi:10.3390/rs10081250.
- Brodersen, K.H., Ong, C.S., Stephan, K.E., Buhmann, J.M., 2010. The balanced accuracy and its posterior distribution. *Proceedings - International Conference on Pattern Recognition*, 3121–3124doi:doi:10.1109/ICPR.2010.764.
- Buades, A., Coll, B., Morel, J.M., 2011. Non-Local Means Denoising. *Image Processing On Line* 1, 208–212. URL: http://www.ipol.im/pub/art/2011/bcm{}_nlm/?utm{}_source=doi, doi:doi:10.5201/ipol.2011.bcm_nlm, arXiv:1112.0311.
- Hamunyela, E., Reiche, J., Verbesselt, J., Herold, M., 2017. Using space-time features to improve detection of forest disturbances from Landsat time series. *Remote Sensing* 9, 1–17. doi:doi:10.3390/rs9060515.
- Hansen, J.N., 2022. nd – a framework for the analysis of n-dimensional earth observation data. *Journal of Open Research Software* 10, 3. URL: <https://doi.org/10.5334/jors.377>, doi:doi:10.5334/jors.377.
- Hansen, J.N., Mitchard, E.T., King, S., 2020. Assessing Forest/Non-Forest Separability Using Sentinel-1 C-Band Synthetic Aperture Radar. *Remote Sensing* 12. doi:doi:10.3390/rs12111899.
- Hansen, M.C., Potapov, P.V., Moore, R., Hancher, M., Turubanova, S.A., Tyukavina, A., Thau, D., Stehman, S.V., Goetz, S.J., Loveland, T.R., Kommareddy, A., Egorov, A., Chini, L., Justice, C.O., Townshend, J.R.G., 2013. High-Resolution Global Maps of 21st-Century Forest Cover Change. *Science* 342, 850–854. doi:doi:10.1126/science.1244693, arXiv:1011.1669v3.

- IPCC, 2003. Good practice guidance for land use, land use change and forestry. Technical Report. URL: <http://www.ipcc-nggip.iges.or.jp>, doi:doi:citeulike-article-id:1260638.
- Kennedy, R.E., Yang, Z., Cohen, W.B., 2010. Detecting trends in forest disturbance and recovery using yearly Landsat time series: 1. LandTrendr - Temporal segmentation algorithms. *Remote Sensing of Environment* 114, 2897–2910. doi:doi:10.1016/j.rse.2010.07.008.
- Lehmann, E.A., Caccetta, P., Lowell, K., Mitchell, A., Zhou, Z.S., Held, A., Milne, T., Tapley, I., 2015. SAR and optical remote sensing: Assessment of complementarity and interoperability in the context of a large-scale operational forest monitoring system. *Remote Sensing of Environment* 156, 335–348. URL: <http://dx.doi.org/10.1016/j.rse.2014.09.034>, doi:doi:10.1016/j.rse.2014.09.034.
- Lu, D., 2006. The potential and challenge of remote sensing-based biomass estimation. *International Journal of Remote Sensing* 27, 1297–1328. doi:doi:10.1080/01431160500486732.
- Mitchard, E.T.A., Saatchi, S.S., Lewis, S.L., Feldpausch, T.R., Woodhouse, I.H., Sonké, B., Rowland, C., Meir, P., 2011. Measuring biomass changes due to woody encroachment and deforestation/degradation in a forest-savanna boundary region of central Africa using multi-temporal L-band radar backscatter. *Remote Sensing of Environment* 115, 2861–2873. URL: <http://dx.doi.org/10.1016/j.rse.2010.02.022>, doi:doi:10.1016/j.rse.2010.02.022.
- Mitchell, A.L., Rosenqvist, A., Mora, B., 2017. Current remote sensing approaches to monitoring forest degradation in support of countries measurement, reporting and verification (MRV) systems for REDD+. *Carbon Balance and Management* 12, 9. URL: <http://cbmjournal.springeropen.com/articles/10.1186/s13021-017-0078-9>, doi:doi:10.1186/s13021-017-0078-9.
- NICFI, 2021. Norway's International Climate and Forest Initiative (NICFI). URL: <https://www.nicfi.no/>.
- Qin, Y., Xiao, X., Wigneron, J.P., Ciais, P., Brandt, M., Fan, L., Li, X., Crowell, S., Wu, X., Doughty, R., Zhang, Y., Liu, F., Sitch, S., Moore, B., 2021. Carbon loss from forest degradation exceeds that from deforestation in the Brazilian Amazon. *Nature Climate Change* 11, 442–448. URL: <http://dx.doi.org/10.1038/s41558-021-01026-5>, doi:doi:10.1038/s41558-021-01026-5.
- Rahman, M.M., Sumantyo, J.T.S., 2010. Mapping tropical forest cover and deforestation using synthetic aperture radar (SAR) images. *Applied Geomatics* 2, 113–121. doi:doi:10.1007/s12518-010-0026-9.
- Reiche, J., Lucas, R., Mitchell, A.L., Verbesselt, J., Hoekman, D.H., Haarpaintner, J., Kellndorfer, J.M., Rosenqvist, A., Lehmann, E.A., Woodcock, C.E., Seifert, F.M., Herold, M., 2016. Combining satellite data for better tropical forest monitoring. *Nature Climate Change* 6, 120–122. URL: <http://dx.doi.org/10.1038/nclimate2919>, doi:doi:10.1038/nclimate2919.
- Rodríguez-Veiga, P., Wheeler, J., Louis, V., Tansey, K., Balzter, H., 2017. Quantifying Forest Biomass Carbon Stocks From Space. *Current Forestry Reports* 3, 1–18. doi:doi:10.1007/s40725-017-0052-5.
- Shimada, M., Itoh, T., Motooka, T., Watanabe, M., Shiraiishi, T., Thapa, R., Lucas, R., 2014. New global forest/non-forest maps from alos palsar data (2007–2010). *Remote Sensing of Environment* 155, 13–31. URL: <https://www.sciencedirect.com/science/article/pii/S0034425714001527>, doi:doi:https://doi.org/10.1016/j.rse.2014.04.014.
- Soja, M.J., Persson, H.J., Ulander, L.M., 2018. Modeling and Detection of Deforestation and Forest Growth in Multitemporal TanDEM-X Data. *IEEE Journal of Selected Topics in Applied Earth Observations and Remote Sensing* 11, 3548–3563. doi:doi:10.1109/JSTARS.2018.2851030.
- Vancutsem, C., Achard, F., Pekel, J.F., Vieilledent, G., Carboni, S., Simonetti, D., Gallego, J., Aragão, L.E., Nasi, R., 2021. Long-term (1990-2019) monitoring of forest cover changes in the humid tropics. *Science Advances* 7, 1–22. doi:doi:10.1126/sciadv.abe1603.
- Verbesselt, J., Hyndman, R., Newnham, G., Culvenor, D., 2010. Detecting trend and seasonal changes in satellite image time series. *Remote Sensing of Environment* 114, 106–115. doi:doi:10.1016/j.rse.2009.08.014.
- Zhu, Z., Woodcock, C.E., 2014. Continuous change detection and classification of land cover using all available Landsat data. *Remote Sensing of Environment* 144, 152–171. doi:doi:10.1016/j.rse.2014.01.011, arXiv:NIHMS150003.
- Zhu, Z., Woodcock, C.E., Olofsson, P., 2012. Continuous monitoring of forest disturbance using all available Landsat imagery. *Remote Sensing of Environment* 122, 75–91. doi:doi:10.1016/j.rse.2011.10.030.